Journal of ELECTRONIC MATERIALS, Vol. 39, No. 10, 2010
DOI: 10.1007/s11664-010-1294-1

High-Performance MWIR/LWIR Dual-Band 640 × 480 HgCdTe/Si FPAs

E.A. PATTEN,[1,2] P.M. GOETZ,[1] M.F. VILELA,[1] K. OLSSON,[1] D.D. LOFGREEN,[1] J.G. VODICKA,[1] and S.M. JOHNSON[1]

1.—Raytheon Vision Systems, 75 Coromar Drive, Goleta, CA 93117, USA. 2.—e-mail: epatten@raytheon.com

HgCdTe grown on large-area Si substrates allows for larger array formats and potentially reduced focal-plane array (FPA) cost compared with smaller, more expensive CdZnTe substrates. The goal of this work is to evaluate the use of HgCdTe/Si for mid-wavelength/long-wavelength infrared (MWIR/LWIR) dual-band FPAs. A series of MWIR/LWIR dual-band HgCdTe triple-layer *n-P-n* heterojunction (TLHJ) device structures were grown by molecular-beam epitaxy (MBE) on 100-mm (211)Si substrates. The wafers showed low macrodefect density (<300 cm^{-2}) and was processed into 20-μm-unit-cell 640 × 480 detector arrays which were mated to dual-band readout integrated circuits (ROICs) to produce FPAs. The measured 80-K cutoff wavelengths were 5.5 μm for MWIR and 9.4 μm for LWIR, respectively. The FPAs exhibited high pixel operabilities in each band, with noise equivalent differential temperature (NEDT) operabilities of 99.98% for the MWIR band and 99.6% for the LWIR band demonstrated at 84 K.

Key words: HgCdTe, dual band, FPAs, Si substrates, infrared detectors, molecular-beam epitaxy (MBE)

INTRODUCTION

HgCdTe epitaxially grown on large-area Si substrates allows IR FPAs to be scaled to larger formats than is possible with the largest (8 cm × 8 cm) CdZnTe substrates presently available. Large Si substrates also allow higher array count per wafer for reduced die cost. Our previous work demonstrated state-of-the-art MWIR FPAs using HgCdTe grown on 100-mm- and 150-mm-diameter (211)Si substrates by MBE.[1] In recent years this work has been extended into the 10 μm to 11 μm LWIR range; however, in this regime, FPA operability begins to degrade as the background flux is lowered.[2,3]

The goal of the work reported herein is to evaluate the use of HgCdTe/Si for MWIR/LWIR dual-band FPAs, as this growth technology has substantial promise for reducing FPA cost. Several groups are exploring MWIR or LWIR HgCdTe grown on large-area substrates (alternatives to CdZnTe), but few have reported work on dual-band FPAs using HgCdTe grown on these substrates. Selex has reported results for MWIR/LWIR FPAs based on HgCdTe grown on GaAs.[4]

A series of MWIR/LWIR dual-band HgCdTe *n-P-n* triple-layer heterojunction device structures were grown on 100-mm (211)Si substrates using ZnTe and CdTe buffer layers. The triple-layer structure used on Si was based on successful structures grown routinely at Raytheon on CdZnTe substrates. The 78-K target cutoff wavelengths were 5.5 μm and 9.4 μm for the MWIR and LWIR bands, respectively. Full-wafer defect maps of these MWIR/LWIR HgCdTe/Si wafers show low macrodefect (voids + microvoids) densities (<300 cm^{-2}).

Several of these layers were processed into 640 × 480 detector arrays and smaller test structure arrays. The fabrication process for these dual-band HgCdTe on Si detectors utilized mature fabrication processes at Raytheon developed and validated for dual-band HgCdTe on CdZnTe. Selected detector

(Received January 22, 2010; accepted May 12, 2010; published online May 29, 2010)

and ROIC arrays were hybridized to fabricate FPAs. The better FPAs of those tested demonstrated NEDT operabilities up to 99.98% for the MWIR band and 99.6% for the LWIR band at 84 K, *f*/2.9 background. These results indicate that heteroepitaxial HgCdTe/Si is beginning to show promise for large-format dual-band FPAs.

DUAL-BAND DETECTOR DESCRIPTION

The current Raytheon dual-band detector is based on a bias-selectable back-to-back diode structure.[5] Our single-mesa architecture for the dual-band detector with its single contact per unit cell is shown in Fig. 1. This detector utilizes an MBE-grown *n*-*P*-*n* triple-layer heterojunction structure. Operated with backside illumination, the bottom *n*-type layer absorbs the shorter-wavelength (band 1) radiation, which is sensed by the bottom photodiode. Longer-wavelength (band 2) radiation passes through the bottom *n*-type absorber and middle p^+ layer and is detected by the top photodiode.

The dual-band mesas are formed using an inductively coupled plasma (ICP) dry-etch process that produces smooth, steep sidewalls. This structure achieves approximately 100% optical fill factor in each band, due to total internal reflection of incident radiation off mesa sidewalls. The high band 2 fill factor of this structure offers advantages over structures that require two contacts per unit cell. Additionally, band 2 is fully reticulated and band 1 is partially reticulated, which minimizes spatial crosstalk between pixels. The polarity of the bias across the structure determines which junction is photoactive and thereby the spectral band of the detector. The bias switching is performed by the dual-band ROIC. As the detector bias is changed from that of one band to the other, the detector current is directed to separate input circuitry and integration capacitors specific to each band. The bias switching can be performed at times much shorter than the frame period using a process known as time-division multiplexed integration (TDMI); this allows the signals from both bands to be interlaced during a single frame. For example, switching times of much less than 1 ms are routinely used for the MWIR/LWIR dual-band FPAs and provide near-simultaneous integration of band 1 and band 2 signals.[6]

MATERIAL GROWTH AND CHARACTERIZATION

The MWIR/LWIR dual-band *n*-*P*-*n* TLHJ HgCdTe structures were grown on 100-mm (211)Si wafers in a Riber Epineat MBE system using CdTe, ZnTe, and Te solid sources and a liquid Hg source. Elemental sources of indium and arsenic were used for *n*-type and *p*-type doping, respectively. The 100-mm Si (211) substrates were prepared for growth using a hydrofluoric-acid-based process. A thin ZnTe nucleation layer followed by a CdTe buffer layer was used as a template for the HgCdTe device layers. Once the Si substrate was introduced, all layers were grown without wafer removal from the MBE system. An overview of heteroepitaxial HgCdTe/Si technology was published earlier.[7]

The layers were characterized using room-temperature Fourier-transform infrared transmission (FTIR) mapping measurements coupled with modeling of the transmission spectra[8] to extract layer thickness and the MWIR (band 1) and LWIR (band 2) cutoff wavelengths projected at 78 K. Macrodefect density was measured using an August Technology NSX105 automated defect inspection system which enables full-wafer mapping.[9] Table I summarizes the FTIR-derived characteristics of four MWIR/LWIR dual-band wafers along with the full-wafer average values of macrodefect density. Overall, the wafer quality was very good, with total

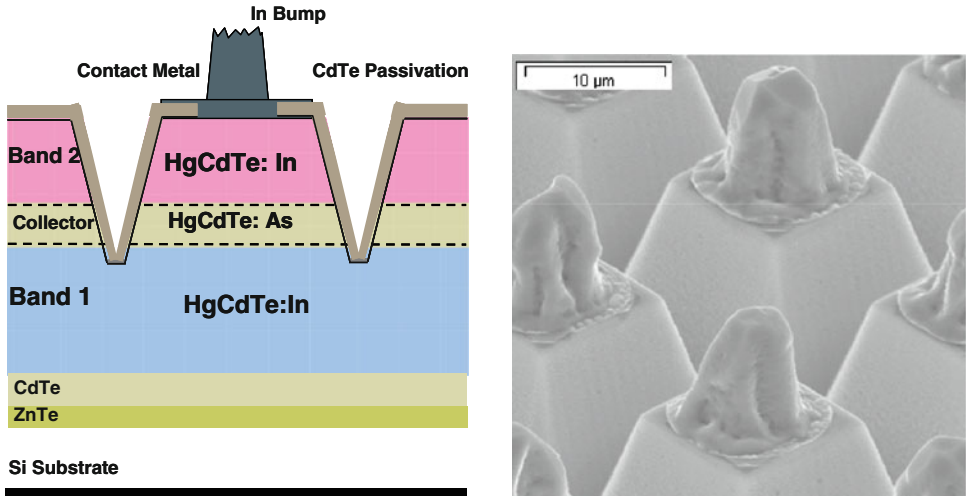

Fig. 1. Cross-section of Raytheon's single-mesa dual-band detector architecture applied to HgCdTe on Si (*left*). Scanning electron micrograph of 20-μm-unit-cell dual-band detectors (*right*).

Table I. Summary of FTIR-derived characteristics of four MWIR/LWIR HgCdTe/Si dual-band wafers along with full-wafer average values of macrodefect density

Wafer ID	78-K Band 1 Cutoff/Photon (μm)	78-K Band 2 Cutoff/Photon (μm)	HgCdTe Thickness (μm)	Microvoid Density (cm^{-2})	Void Density (cm^{-2})	Total Macrodefect Density (cm^{-2})
3-2609	5.11	9.17	14.3	234	123	357
3-2610	5.19	9.40	15.5	166	97	263
3-2614	5.33	9.31	14.3	175	74	249
3-2615	5.31	9.22	14.9	185	91	276

MWIR/LWIR HgCdTe/Si dual-band wafers had low defect density and were selected for processing into dual-band detector arrays.

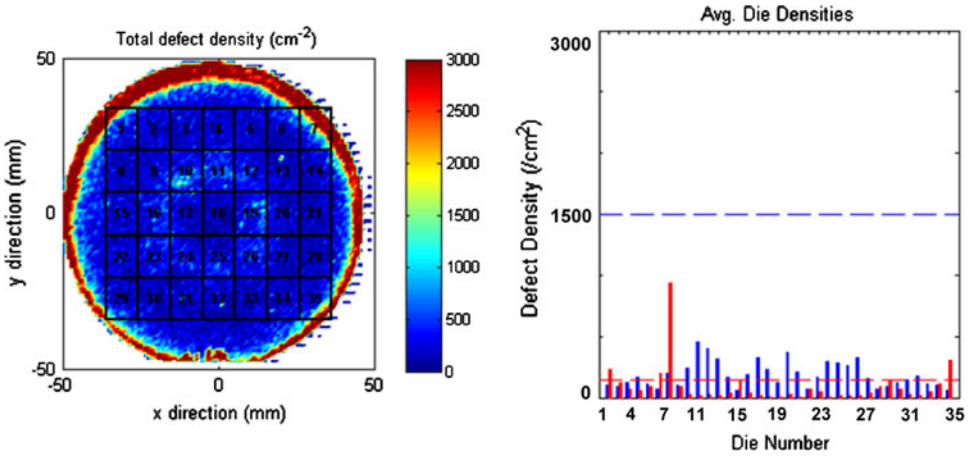

Fig. 2. Full-wafer defect map of a 100-mm-diameter MWIR/LWIR HgCdTe/Si dual-band wafer (3-2615) along with statistics of individual 640 × 480, 20-μm-sized dies overlaid on the defect map. Macrodefect densities for this wafer averaged <300 cm^{-2}.

macrodefect densities <300 cm^{-2}. Figure 2 shows an August defect map of one of these wafers along with the defect statistics of individual virtual arrays (20 μm, 640 × 480) overlaid on the map.

ARRAY FABRICATION AND TEST

Several MWIR/LWIR dual-band HgCdTe/Si layers were processed into 20-μm-unit-cell 640 × 480 detector arrays and small test structure arrays. A representative dual-band detector is shown in Fig. 1. Detector fabrication began with mesa delineation of individual pixels using ICP dry etching, followed by deposition and patterning of surface passivation, contact metal, and indium bumps. At the end of wafer processing, the individual detector arrays were diced from each wafer and hybridized to dual-band Si ROIC arrays to form dual-band FPAs. Smaller detector test arrays (20 μm unit cell) were hybridized to sapphire fanout boards to form test structure assemblies (TSAs) for direct testing of detector performance in a cryogenic Dewar (current–voltage and spectral response).

Example 80-K current–voltage curves and spectral response data for MWIR/LWIR HgCdTe/Si detectors from a TSA are shown in Fig. 3. The current–voltage data show the expected serpentine shape for back-to-back diodes. These curves are obtained by sweeping the bias polarity of the pixel contact from negative to positive. The MWIR junction is photoactive when the applied bias is negative, and the LWIR junction is photoactive when the applied bias is greater than approximately 150 mV. Note that this is the bias applied to the stacked diode structure and not the bias across an individual junction. The spectral response curves were obtained by setting the bias for MWIR (negative voltage) and repeating a separate measurement at the LWIR bias to obtain data such as shown in Fig. 3. For these MWIR/LWIR detectors, the average cutoff wavelengths for the two bands were 5.5 μm for MWIR and 9.4 μm for LWIR, which met the targets set for MBE growth of these layers.

The 640 × 480 FPAs were evaluated at 84 K in a laboratory Dewar with a dual-band cold filter defining the MWIR and LWIR spectral bands. FPAs were operated with integration times that were roughly consistent with 60 Hz operation. FPA output levels were measured for blackbody temperatures (background) of 300 K and 305 K. Data

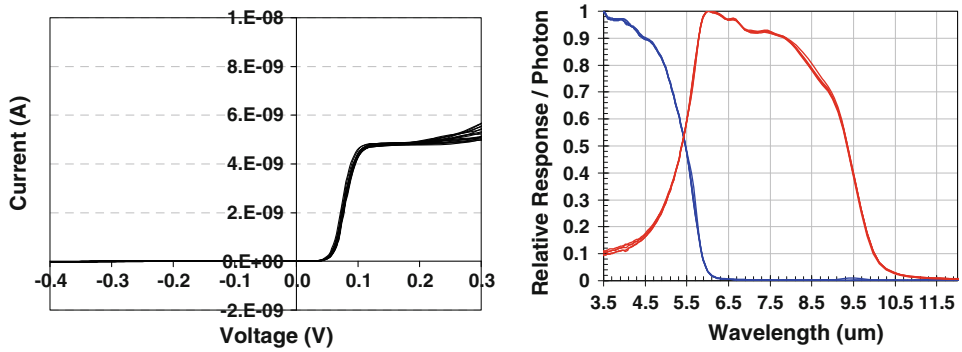

Fig. 3. Example of 80-K, *f*/2 field-of-view, current–voltage characteristics (*left*) and spectral response data (*right*) for 20-μm-unit-cell MWIR/LWIR HgCdTe/Si detectors in a hybridized test structure. The current–voltage data show the expected serpentine shape for back-to-back diodes (MWIR for negative bias, LWIR for voltage >100 mV). The average cutoff wavelengths for the two bands were 5.5 μm for MWIR band and 9.4 μm for LWIR band.

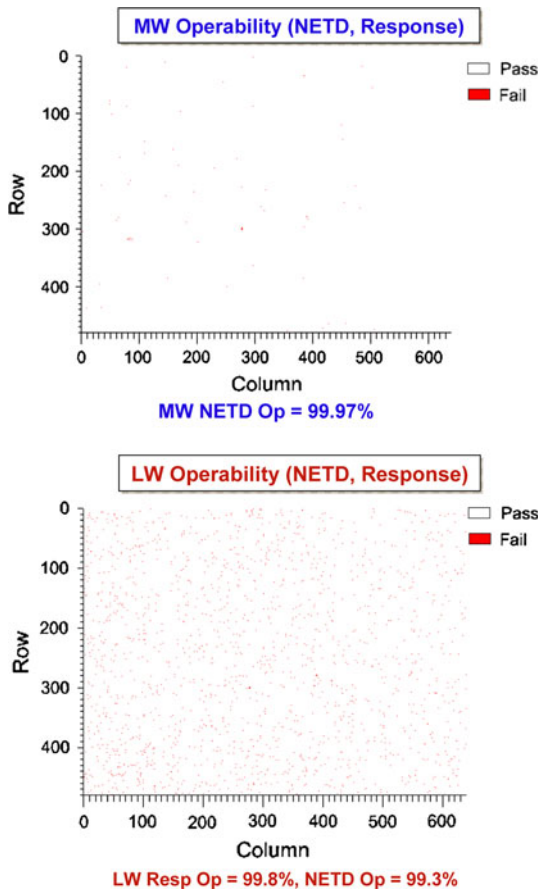

Fig. 4. Operability maps for the two bands (MWIR at *top*, LWIR at *bottom*) of an MWIR/LWIR HgCdTe on Si FPA. These operability maps include all NETD and response defects. The FPA was operated at 84 K nominal in a laboratory test Dewar with *f*/3.5 field of view. This FPA, as well as others produced, showed high pixel operabilities in both bands with no significant cluster defects. The low numbers of inoperable pixels occur in a random "salt and pepper" distribution.

were taken with both *f*/3.5 and *f*/2.9 apertures. Example data for these FPAs are shown in Figs. 4, 5, and 6. Figure 4 shows NETD operability maps for the MWIR and LWIR bands of one of these FPAs. For the NETD operabilities, operable pixels were defined as those having NETD <112 mK. The calculated response operabilities were based upon a 3:1 pixel responsivity ratio window. The MWIR operability was 99.97% (84 K, *f*/3.5 background), with LWIR operability of 99.3% under the same conditions. NETD histograms for this FPA are shown in Fig. 5. The MWIR has a very tight distribution, while a tail in the LWIR distribution at higher NETD values (noise tail) is observed. There is currently not a detailed understanding for the mechanisms leading to the higher-noise LWIR pixels in the tail of the distribution. These poorer pixels do not appear to correlate directly with the uniform dislocation density measured in these materials. Efforts are underway to understand the detailed physical mechanisms for these poorer-performing pixels.[10] Increasing the background flux by measuring at *f*/2.9 field-of-view improves the LWIR NETD characteristics significantly, as shown in Fig. 6, with LWIR NETD operability of 99.6% demonstrated (corresponding LWIR response operability was 99.9%).

CONCLUSIONS

MWIR/LWIR dual-band HgCdTe/Si 640×480 FPA results from Raytheon are reported for the first time. A series of MWIR/LWIR dual-band HgCdTe triple-layer *n*-*P*-*n* heterojunction device structures was grown by MBE on 100-mm (211)Si substrates. The wafers showed low macrodefect density (<300 cm^{-2}) and were processed into 20-μm-unit-cell 640×480 detector arrays and small test structure arrays. Hybridized detector test structure arrays showed classic dual-band back-to-back diode current–voltage characteristics and 80-K cutoff wavelengths of 5.5 μm for MWIR and 9.4 μm for LWIR. Selected 640×480 detector arrays were mated to dual-band ROICs to produce FPAs. The FPAs exhibited high pixel operabilities in each band, with NETD operabilities up to 99.98% for the MWIR band and 99.6% for the LWIR band at

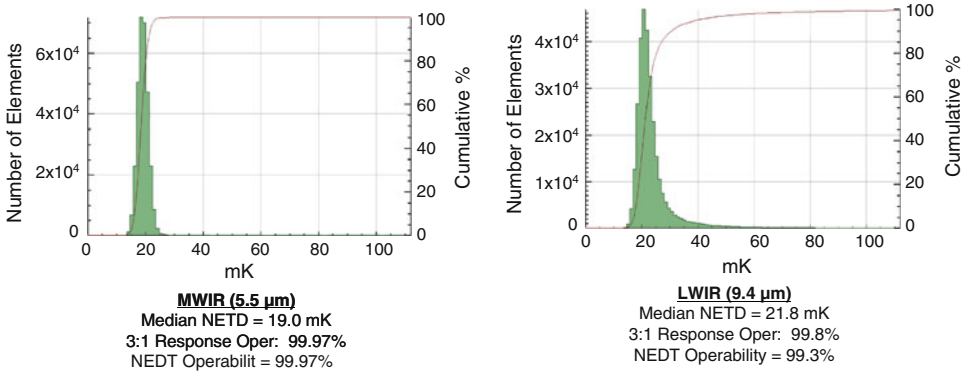

Fig. 5. NEDT histograms for the MWIR band (*left*) and the LWIR band (*right*) of a 640 × 480 MWIR/LWIR dual-band HgCdTe/Si FPA tested at 84 K, *f*/3.5 field of view, 300 K background.

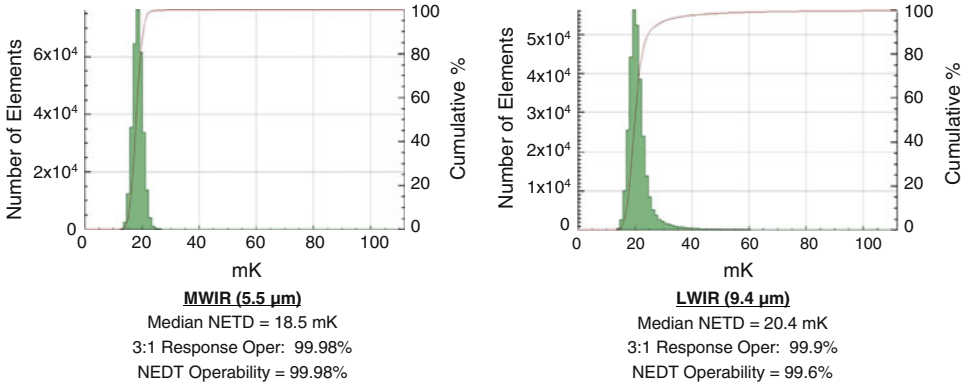

Fig. 6. NEDT histograms for the MWIR band (*left*) and the LWIR band (*right*) of a 640 × 480 MWIR/LWIR dual-band HgCdTe/Si FPA tested at 84 K, *f*/2.9 field of view, 300 K background.

84 K, *f*/2.9 background (with corresponding LWIR response operabilities as high as 99.9%). These results validate the high quality of Raytheon's HgCdTe/Si dual-band material and indicate that heteroepitaxial HgCdTe/Si is beginning to show promise for large-format dual-band FPAs. Work will continue towards understanding what limits the operability of the LWIR band with the goal of a higher-yield, lower-cost dual-band technology for the future.

REFERENCES

1. E.P.G. Smith, R.E. Bornfreund, I. Kasai, L.T. Pham, E.A. Patten, J.M. Peterson, J.A. Roth, B.Z. Nosho, T.J. de Lyon, J.E. Jensen, J.W. Bangs, S.M. Johnson, and W.A. Radford, *Proc. SPIE* 6127, 61271F (2006).
2. R. Bornfreund, J.P. Rosbeck, Y.N. Thai, E.P. Smith, D.D. Lofgreen, M.F. Vilela, A.A. Buell, M.D. Newton, K. Kosai, S.M. Johnson, T.J. de Lyon, J.E. Jensen, and M.Z. Tidrow, *J. Electron. Mater.* 36, 1085 (2007).
3. M.F. Vilela, D.D. Lofgreen, E.P.G. Smith, M.D. Newton, G.M. Venzor, J.M. Peterson, J.J. Franklin, M. Reddy, Y. Thai, E.A. Patten, S.M. Johnson, and M.Z. Tidrow, *J. Electron. Mater.* 37, 1465 (2008).
4. C.L. Jones, L.G. Hipwood, J. Price, C.J. Shaw, P. Abbott, C.D. Maxey, H.W. Lau, R.A. Catchpole, M. Ordish, P. Knowles, and N.T. Gordon, *Proc. SPIE* 6542, 654210 (2007).
5. W.A. Radford, E.A. Patten, D.F. King, G.K. Pierce, J. Vodicka, P. Goetz, G. Venzor, E.P.G. Smith, R. Graham, S.M. Johnson, J. Roth, B. Nosho, and J. Jensen, *Proc. SPIE* 5783, 331 (2005).
6. D.F. King, W.A. Radford, E.A. Patten, R.W. Graham, T.F. McEwan, J.G. Vodicka, R.E. Bornfreund, P.M. Goetz, G.M. Venzor, S.M. Johnson, J.E. Jensen, B.Z. Nosho, and J.A. Roth, *Proc. SPIE* 6206, 62060W-1 (2006).
7. S.M. Johnson, W.A. Radford, A.A. Buell, M.F. Vilela, J.M. Peterson, J.J. Franklin, R.E. Bornfreund, A.C. Childs, G.M. Venzor, M.D. Newton, E.P.G. Smith, L.M. Ruzicka, G.K. Pierce, D.D. Lofgreen, T.J. de Lyon, and J.E. Jensen, *Proc. SPIE* 5732, 250 (2005).
8. D.D. Lofgreen, C.M. Peterson, A.A. Buell, M.F. Vilela, and S.M. Johnson, *J. Electron. Mater.* 35, 1487 (2006).
9. D.D. Lofgreen, M.F. Vilela, E.P. Smith, M.D. Newton, D. Beard, and S.M. Johnson, *J. Electron. Mater.* 36, 958 (2007).
10. J.D. Benson, L.O. Bubulac, P.J. Smith, R.N. Jacobs, J.K. Markunas, M. Jaime-Vasquez, L.A. Almeida, A. Stoltz, P.S. Wijewarnasuriya, G. Brill, Y. Chen, U. Lee, M.F. Vilela, J. Peterson, S.M. Johnson, D.D. Lofgreen, D. Rhiger, E.A. Patten, and P.M. Goetz, *J. Electron. Mater.* (2010) at these proceedings.